ELSEVIER

Fusion Engineering and Design 32–33 (1996) 569–576

Fusion Engineering and Design

On the gain scaling of ICF targets

Mikhail M. Basko

Institute for Theoretical and Experimental Physics, B. Cheremushkinskaya 25, 117259 Moscow, Russia

Abstract

A new gain model based on a adiabatic self-similar solution of the hydrodynamic equations is proposed for deuterium–tritium fusion capsules ignited by means of a thermonuclear spark at the fuel center. The model is applied to analyze gain curves that correspond to fixed values of the implosion velocity U_{im}. It is shown that the threshold energy investment into the fuel required for ignition scales as $E_{\mathrm{f,min}} \propto \alpha^3 U_{\mathrm{im}}^{-7}$ for capsules with initially thin shells, i.e. when the initial aspect ratio $A_0 \gg 1$. In the opposite limit of initially thick capsule shells, the scaling of $E_{\mathrm{f,min}}$ with the entropy parameter α and the implosion velocity U_{im}, and that of the limiting fuel gain G_{f}^* with E_{f} become ill defined; nevertheless, a fair agreement with the Livermore results is observed for α values between 1 and 2, and $U_{\mathrm{im}} \approx 4 \times 10^7\ \mathrm{cm\ s^{-2}}$.

1. Introduction

The prospects for inertial confinement fusion (ICF) are often discussed by invoking the plots of the target energy gain G versus the input driver energy E_{dr}. Alluding to sophisticated numerical simulations, the Livermore group has quoted the scaling $E_{\mathrm{dr,min}} \propto \alpha^{1.5} U_{\mathrm{im}}^{-5}$ for the ignition energy threshold $E_{\mathrm{dr,min}}$ as a function of the implosion velocity U_{im} and the cold fuel entropy parameter α, and $G^* \propto E_{\mathrm{dr}}^{0.73}$ for the limiting gain G^* [1]. These scalings differ significantly from the relationships $E_{\mathrm{dr,min}} \propto \alpha^3 U_{\mathrm{im}}^{-10}$ and $G^* \propto E_{\mathrm{dr}}^{0.32}$ established in the framework of the isobaric gain model, based on the analysis of the deuterium–tritium fuel states at the time of stagnation [2,3].

The semi-analytical gain model proposed here is also based on the analysis of the assembled fuel configurations and includes three new features: (i) it employs a self-similar solution of the hydrodynamic equations to approximate the density and pressure profiles in the imploding fuel near the time of ignition; (ii) it incorporates an adequate scaling $\rho_{\mathrm{s}} R_{\mathrm{s}} T_{\mathrm{s}} \propto U_{\mathrm{im}}$ for the product of the spark areal density $\rho_{\mathrm{s}} R_{\mathrm{s}}$ by its temperature T_s at the ignition threshold — as contrasted to fixed values of $\rho_s R_s$ and T_{s} used by the most of the previous authors; (iii) the constraints that result from the drive asymmetries and hydrodynamic instabilities are taken into account as certain fixed values of the capsule radial convergence ratio C_0 and the fuel shell in flight aspect ratio A_{c}. It should be noted that Atzeni [4] and Meyer-ter-Vehn et al. [5] have already attempted to incorporate the asymmetry and instability constraints into the isobaric gain model and, as a consequence, found an improved agreement with the Livermore results. However, in contrast to the present work, these authors assumed fixed values of the initial rather than the in flight aspect ratios of the fuel shell.

PII S0920-3796(96)00517-0

As a consequence of the new elements listed above, our model predicts the scalings $E_{\mathrm{dr,min}} \propto \alpha^3 U_{\mathrm{im}}^{-7}$ and $G^* \propto (E_{\mathrm{dr}}/\alpha^3)^{0.4}$, provided that a fixed coupling efficiency between the driver energy E_{dr} and the fuel energy E_{f} is assumed. The scalings apply in the most favorable case when the initial thickness of the fusion capsule is small compared with its initial radius (the initial aspect ratio $A_0 \gg 1$). In the opposite limit of initially thick capsule shell, the scalings of $E_{\mathrm{dr,min}}$ with U_{im} and α, and of G^* with E_{dr} and α become ill defined; neverthless, a fair agreement between the predictions of the present model and the recent Livermore results [1] is observed for initially thick capsule shells in a limited range of parameters, at the values of α somewhere between 1 and 2, and $U_{\mathrm{im}} \approx 4 \times 10^7\ \mathrm{cm\ s^{-1}}$.

2. Fuel parametrization

To obtain a suitable parametrization of possible DT fuel configurations near the time of ignition, we invoke the self-similar solution

$$r = \xi R(t) \tag{1}$$

$$u(t, r) = \dot{R}\xi \tag{2}$$

$$\rho(t, r) = \rho_0(t)\omega(\xi) \tag{3}$$

$$P(t, r) = P_0(t)\left[1 - \frac{1}{\Omega}\int_0^{\xi} \xi'\omega(\xi')\,\mathrm{d}\xi'\right] \tag{4}$$

which describes a homologous adiabatic contraction (expansion) of a gaseous sphere of radius $R(t)$ with a prescribed entropy distribution over the mass coordinate. Here, ξ is the self-similar variable, $\omega(\xi)$ is an arbitrary function that defines the DT density (or, equivalently, entropy) profile over the mass coordinate, and

$$\Omega = \int_0^1 \xi\omega\,\mathrm{d}\xi \tag{5}$$

is a dimensionless constant. One can readily verify by a straightforward substitution that Eqs. (1)–(4) satisfy the equations of one-dimensional hydrodynamics for spherical motions of a gas with an adiabatic index of $\frac{5}{3}$, provided that the combinations $\rho_0(t)R^3(t)$ and $P_0(t)/\rho_0^{5/3}(t)$ remain constant, and

$$R(t) = (R_{\mathrm{m}}^2 + U_\infty^2 t^2)^{1/2} \tag{6}$$

Here, R_{m} is the fuel radius at the time of stagnation $t = 0$, and U_∞ is the implosion velocity of the outer fuel edge in the limit of $t \to -\infty$.

For subsequent calculations, we adopt the dimensionless density profile $\omega(\xi)$ such that (i) the fuel density is constant over the central hot spot $0 < \xi < \xi_{\mathrm{s}}$, and (ii) the cold fuel layer at $\xi_{\mathrm{s}} < \xi < 1$ has a constant value of the entropy parameter $\alpha \equiv P(t, r)/P_{\mathrm{deg}}(t, r) \propto P/\rho^{5/3}$, where $P_{\mathrm{deg}}[\mathrm{Mbar}] = 2.18\,(\rho[\mathrm{g\ cm^{-3}}])^{5/3}$ is the cold pressure of the degenerate electron gas in a fully ionized equimolar DT mixture of density ρ. Combined with Eq. (5), the latter two conditions lead to the expression

$$\omega(\xi) = \begin{cases} 1, & 0 < \xi < \xi_{\mathrm{s}} \\ 5\dfrac{\Omega - \frac{1}{2}\xi_{\mathrm{s}}^2}{(1 - \xi_{\mathrm{s}}^2)^{5/2}}(1 - \xi^2)^{3/2}, & \xi_{\mathrm{s}} < \xi < 1 \end{cases} \tag{7}$$

which was used in all the calculations below.

Here, it should be emphasized that the adiabatic solution of Eqs. (1)–(6) is employed to approximate not the entire process of the fuel implosion but, rather, its motion during a short period just prior to ignition, within which the effects of non-adiabatic process do not have time to accumulate and cause serious flow distortions.

In the framework of our scheme, the DT fuel configuration at the time of stagnation ($t = 0$) is fully specified by the values of the parameters in Table 1.

The velocity U_∞ in Eq. (6) differs from what is usually meant as the implosion velocity U_{im}. We relate U_{im} to U_∞ by assuming that the kinetic energy of the cold fuel in the limit $t \to -\infty$ is $\frac{1}{2}M_{\mathrm{c}}U_{\mathrm{im}}^2$, where M_{c} is the cold fuel mass at $\xi_{\mathrm{s}} < \xi < 1$. As a result, one calculates

Table 1
Parameters used in present framework

$U_{\mathrm{im}}(10^7\ \mathrm{cm\ s^{-1}})$	the implosion velocity
T_{s} (keV)	the central spark temperature
$H_{\mathrm{s}} \equiv \rho_{\mathrm{s}}\mathrm{R}_{\mathrm{s}}$ (g cm^{-2})	the spark $\langle\rho r\rangle$
$\alpha = P/P_{\mathrm{deg}}$	the entropy parameter
$\xi_{\mathrm{s}} = \mathrm{R}_{\mathrm{s}}/\mathrm{R}_{\mathrm{f}}$	the fractional spark radius

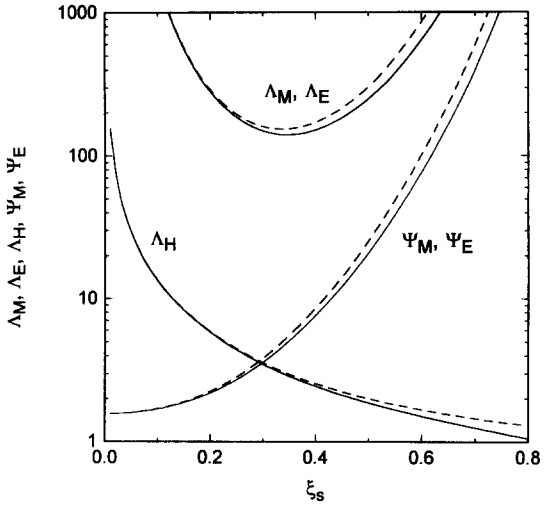

Fig. 1. Dimensionless functions $\Lambda_M(\Omega, \xi_s)$, $\Lambda_E(\Omega, \xi_s)$, $\Lambda_H(\Omega, \xi_s)$, $\Psi_M(\Omega, \xi_s)$ and $\Psi_E(\Omega, \xi_s)$ plotted versus fractional spark radius ξ_s for two values of Ω:—, $\Omega = 1$;– – –, $\Omega = 2$. In both cases, Λ_M coincides with Λ_E, and Ψ_M coincides with Ψ_E within the thickness of corresponding curves.

$$\frac{U_\alpha}{U_{im}} = \left(\frac{8}{3}\frac{\phi_M}{\phi_E}\right)^{1/2}$$

$$\Omega = 2.9\,\frac{T_s}{U_{im}^2}\,\frac{\phi_E}{\phi_M} \tag{8}$$

where

$$\phi_M = \frac{\pi/2 - \arcsin\xi_s}{(1-\xi_s^2)^{5/2}} + \frac{\xi_s}{3}\,\frac{8\xi_s^4 - 14\xi_s^2 + 3}{(1-\xi_s^2)^2} \tag{9}$$

$$\phi_E = \frac{\pi/2 - \arcsin\xi_s}{(1-\xi_s^2)^{5/2}} + \frac{\xi_s}{3}\,\frac{16\xi_s^6 - 24\xi_s^4 + 2\xi_s^2 + 3}{(1-\xi_s^2)^2} \tag{10}$$

In terms of our basic parameters in Table 1, the fuel density in the spark region is

$$\rho_s[\mathrm{g\ cm^{-3}}] = 8.36\,\frac{U_{im}^5}{\alpha^{3/2}T_s}\,\frac{(1-\xi_s^2)^{5/2}}{1-(2\Omega)^{-1}\xi_s^2}\left(\frac{\phi_M}{\phi_E}\right)^{5/2} \tag{11}$$

while the total mass M_f and the energy E_f of the fuel are given by

$$M_f[\mathrm{mg}] = 163\,\frac{\alpha^3(H_sT_s)_3}{U_{im}^{12}}\,\Lambda_M(\Omega, \xi_s) \tag{12}$$

$$E_f[\mathrm{kJ}] = 813\,\frac{\alpha^3(H_sT_s)^3}{U_{im}^{10}}\,\Lambda_E(\Omega, \xi_s) \tag{13}$$

Here, $\Lambda_M(\Omega, \xi_s)$ and $\Lambda_E(\Omega, \xi_s)$ are analytical functions of Ω and ξ_s (for more details, see ref. [6]), whose dependence on ξ_s is shown in Fig. 1. These functions depend very weakly on Ω and practically coincide with one another in the parameter region of interest here; they both achieve minima $\Lambda_{M,min} \approx \Lambda_{E,min} = \Lambda_M \approx 150$ at $\xi_s \approx 0.34$.

If we now assume—as has often been done in simple gain models based on the analysis of the fuel states near ignition—that the ignition threshold is defined by a certain fixed value $H_sT_s = \langle\rho RT\rangle_0$ of the spark $\langle\rho RT\rangle$, which is independent of the other parameters (Table 1) of the model, then we draw the following conclusions from Eqs. (12) and (13):

(i) the most economical regime of ignition, where one can ignite a maximum fuel mass M_f for a given energy E_f, occurs at $\xi_s \approx 0.34$, where $\Lambda_E(\xi_s)$ is a minimum;
(ii) the ignition threshold for the energy E_f invested into the fuel scales as $E_{f,min} \propto \alpha^3 U_{im}^{-10}\rho$ exactly as was derived by Murakami and Meyer-ter-Vehn [3] in the isobaric approximation.

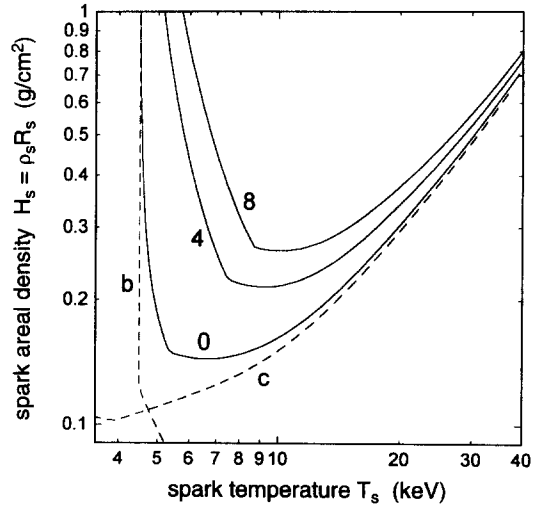

Fig. 2. The full curves show three ignition boundaries for spark parameters as defined by Eq. (17) for three different values (0, 4, and 8) of the right-hand side of this equation (in units of 10^7 cm s^{-1}). To the right hand side of the dashed curve b, the alpha-particle heating Q_α exceeds the bremsstrahlung cooling Q_{br}. Above the dashed curve c, the alpha-particle heating Q_α exceeds the heat conduction cooling Q_{ec}.

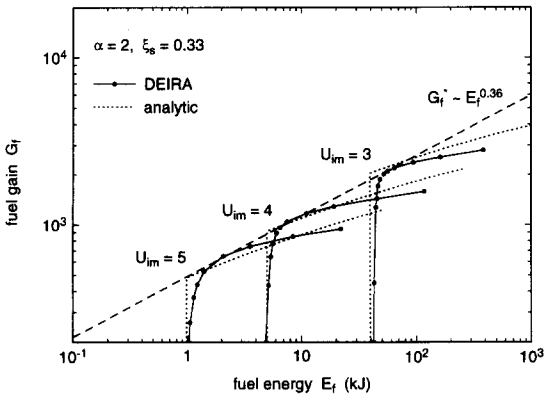

Fig. 3. Gain curves calculated for three implosion velocities with one-dimensional code DEIRA, by varying H_s for fixed $T_s = 7$ keV and $\xi_s = 0.33$. Also shown are the analytic results (· · ·) obtained with the aid of the ignition condition of Eq. (18), and the limiting fuel gain G_f^* (— — —).

A major disagreement of this latter scaling with the Livermore results is in the value of the U_{im} exponent; according to the refs. [1,7], this exponent must be -5 instead of -10. In the next section, we demonstrate that this disagreement is largely explained by inadequate use of the fixed value of H_sT_s as the ignition condition.

The physical reason for the inadequacy of the $H_sT_s = \text{constant}$ ignition condition can be inferred from the expression

$$H_c[\text{g cm}^{-2}] = 5.43\,\frac{H_sT_s}{U_{im}^2}\,\Lambda_H(\Omega, \xi_s) \tag{14}$$

for the areal density H_c of the cold fuel in terms of the basic parameters of Table 1. Here, Λ_H is another analytical function of Ω and ξ_s, which depends very weakly on Ω and whose dependence on ξ_s is illustrated in Fig. 1. Eq. (14) shows that the cold fuel $\langle\rho\Delta r\rangle$—and hence, its tamping effect for the inertial confinement of the fuel assembly—decreases with increasing U_{im}. Therefore, one would expect that the ignition threshold for higher implosion velocities should correspond to higher values of the product H_sT_s.

3. Ignition criterion and basic scaling relationships

First, from Eq. (6), we readily infer the effective time of inertial confinement around the moment of stagnation $t = 0$:

$$\Delta t_c \simeq \frac{R_m}{U_\infty} = \frac{H_s}{\rho_s U_{im}\xi_s}\left(\frac{3}{8}\frac{\phi_E}{\phi_M}\right)^{1/2} \tag{15}$$

For the DT fuel in the spark to undergo a thermonuclear flare, the net energy release during the period of confinement should become at least comparable with the initial energy content in the spark region. Assuming flat temperature and density profiles across the spark region, and taking into account the relevant heating and cooling mechanisms, we can approximately express this condition in the form of the following local relationship at the spark center:

$$(Q_\alpha - Q_{br} - Q_{ec})\Delta t_c \gtrsim \tfrac{3}{2}(n_D + n_T + n_e)T_s \tag{16}$$

where, $Q_\alpha[\text{erg cm}^{-3}\,\text{s}^{-1}] = 8.18 \times 10^{40} f_\alpha \rho_s^2 \langle\sigma v\rangle_{DT}$ is the alpha-particle heating rate (ρ_s is in g cm^{-1} and $\langle\sigma v\rangle_{DT}$ in cm^3 s); Q_{br} and Q_{ec} are respectively the bremsstrahlung and the electron heat conduction cooling rates; and f_α is the reduction factor that results from escape of alpha particles. For subsequent discussion, it will be convenient to rewrite Eq. (16) in the form

$$4.33 \times 10^{18}\frac{f_\alpha\langle\sigma v\rangle_{DT}}{T_s^3}\left(1 - \frac{Q_{br}}{Q_\alpha} - \frac{Q_{ec}}{Q_\alpha}\right)H_sT_s \gtrsim U_{im}\xi_s\left(\frac{\phi_M}{\phi_E}\right)^{1/2} \tag{17}$$

Next, we notice that the left-hand side of Eq. (17) is a function of T_s and H_s only (as long as the weak dependence of Coulomb logarithms on ρ_s can be ignored), while its right-hand side depends exclusively on U_{im} and ξ_s. Thus, for any pair of the U_{im} and ξ_s values, Eq. (17) defines an ignition boundary in the T_s, H_s parametric plane (full curves in Fig. 2). Ignoring for the moment the weak function $(\phi_M/\phi_E)^{1/2}$, we can distinguish two limiting cases with respect to the values of the product $U_{im}\xi_s$, i.e. the limit with $U_{im}\xi_s \ll 10^7$ cm s^{-1} and that with $U_{im}\xi_s \gg 10^7$ cm s^{-1}. In the limit of prolonged confinement, when $U_{im}\xi_s \ll 10^7$

cm s^{-1}, the ignition criterion of Eq. (16) becomes independent of the confinement time Δt_c. The resulting ignition boundary (shown as curve 0 in Fig. 2) is defined by the static condition $Q_\alpha = Q_{br} + Q_{ec}$ and has two branches: a radiative branch, approaching the dashed curve b along which $Q_\alpha = Q_{br}$; and a heat conduction branch, approaching the dashed curve c along which $Q_\alpha = Q_{ec}$. The minimum value of the product $H_s T_s$ along curve 0 corresponds to an absolute ignition threshold with respect to the spark $\langle \rho RT \rangle$ value, which applies in the limit of $U_{im}\xi_s = 0$.

In the opposite limit of high implosion velocites, i.e. $U_{im}\xi_s \gg 10^7$ cm s^{-1}, implying short confinement times, the ignition criterion of Eq. (16) becomes strongly dynamic and is controlled primarily by the finite confinement time Δt_c. In Fig. 2, it is clearly seen that the threshold values of $H_s T_s$ calculated along the ignition boundaries with high values of $U_{im}\xi_s$ (curves labelled as 4 and 8) move up and away from both the radiative (dashed curve b) and the heat conduction (dashed curve c) brances. Hence, the ignition threshold in the inertial limit of $U_{im}\xi_s \gg 10^7$ cm s^{-1} can be evaluated by assuming $Q_{br} \ll Q_\alpha$, $Q_{ec} \ll Q_\alpha$, and asymptotically—as one readily verifies from Eq.

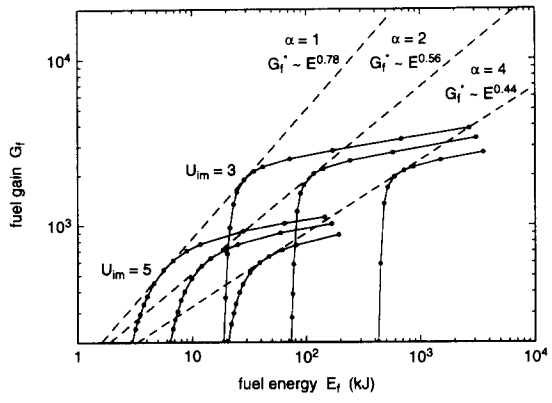

Fig. 4. Three families of gain curves calculated with the DEIRA code for three values of the entropy parameter α. Each gain curve has its own value of the fractional spark radius ξ_s calculated from Eqs. (25) and (26) for fixed values of the fuel in-flight aspect ratio $A_c = 30$ and the capsule convergence ratio $C_0 = 30$. For different values of α, we obtain different scalings of the limiting fuel gain G_f^* with the input energy E_f (dashed lines).

(17)—the threshold value $\langle \rho RT \rangle_0$ becomes directly proportional to the product $U_{im}\xi_s(\phi_M/\phi_E)^{1/2}$.

Clearly, the above analysis based on Eq. (16) is only semi-quantitative. To find out precisely what ignition regime pertains to situations of practical interest, a series of one-dimensional hydrodynamic simulations, starting at the time of stagnation, has been carried out with the one-dimensional three-temperature code DEIRA, which includes all basic physics relevant for spark ignition. The intial state of the DT sphere in each numerical run was assigned according to the self-similar solution of Eqs. (1)–(6) at time $t = 0$. These simulations have unequivocally demonstrated that, for spark temperatures $7 \lesssim T_s \lesssim 12$ keV, the ignition threshold $\langle \rho RT \rangle_0$ is directly proportional to the implosion velocity U_{im}, when $U_{im} \geqslant 3 \times 10^7$ cm s^{-1} and $\xi_s \gtrsim 0.25$. On evaluating the proportionality factor from the numerical simulations, we arrive at the ignition criterion

$$T_s \gtrsim 7 \text{ keV}$$

$$H_s T_s [\text{g cm}^{-1} \text{ keV}] \geqslant \langle \rho RT \rangle_0 \approx 1.4 U_{im}\xi_s \left(\frac{\phi_M}{\phi_E}\right)^{1/2} \quad (18)$$

In other words, within the parameter range of interest here, the ignition criterion is controlled by the finite confinement rather than by the bremstrahlung and heat conduction losses from the thermonuclear spark.

On substituting the ignition threshold for $H_s T_s$ as given by Eq. (18) into Eqs. (12) and (13), we obtain the following expressions for the minimum mass and energy of the DT fuel that can be ignited at a given implosion velocity:

$$M_{f,min}[\text{mg}] = 446 \frac{\alpha^3}{U_{im}^9} \Psi_M(\Omega, \xi_s) \quad (19)$$

$$E_{f,min}[\text{kJ}] = 2.23 \times 10^3 \frac{\alpha^3}{U_{im}^7} \Psi_E(\Omega, \xi_s) \quad (20)$$

The analytical functions $\Psi_M(\Omega, \xi_s)$ and $\Psi_E(\Omega, \xi_s)$ (for explicit expressions, see Ref. [6]) are shown in Fig. 1. They practically coincide with one another and depend only very weakly on Ω. It should be noted that, in realiy, the ignition threshold $E_{f,min}$

does not increase monotoncially with ξ_s, as is shown in Fig. 1; instead it has a minimum at $\xi_s \simeq 0.3$, because the ignition condition of Eq. (18) becomes inadequate at $\xi_s \simeq 0.2$.

Eqs. (19) and (20) represent the scaling laws in the most favorable case, governed exclusively by the thermonuclear ignition physics, when no additional constraints from, say, the hydrodynamic instabilities, fuel preheat, etc., are imposed on the fuel implosion. As shown in Fig. 3, these relationships are very well confirmed by the one-dimensional simulations and lead to the following scaling of the limiting fuel energy gain:

$$G_f^* \propto (E_f/\alpha^3)^{0.36} \tag{21}$$

Although this result is hardly distinguishable from the G_f^* scaling obtained by Meyer-ter-Vehn [2] in the isobaric model, the scaling of Eq. (20) is quite distinct from the $E_{f,min} \propto \alpha^3 U_{im}^{-10}$ law derived by Murakami and Meyer-ter-Vehn [3] within the same isobaric model.

4. The effect of instablility and asymmetry constraints

Here, we consider how the basic scaling relationships in Eqs. (19)–(21) are affected by additional constraints from the Rayleigh–Taylor instability of ablative acceleration and the large-scale non-uniformities in the driving pressure. To perform the necessary estimates, we have to make certain assumptions for the implosion scheme. Considering fusion capsules driven by thermal X-rays, we assume that a DT shell of mass M_c in the initial solid state is surrounded by an ablator of mass M_a. Let R_0 be the initial outer radius of the ablator and R_1 the initial inner radius of the solid DT shell. Let us also suppose that the implosion occurs in the hydrodynamically most efficient way, i.e. all the ablator mass is evaporated by the end of the implosion and the hydrodynamic efficiency is near its maximum value.

We shall distinguish two phases of the implosion: the prepulse phase and the main pluse phase. In the prepulse phase, the driving pressure rises from its initial level to the peak value in such a way as to set the DT shell on the required isentrope with a given value of the parameter α. It is assumed that, by the end of this phase, the inner edge of the fuel shell remains at practically its initial position $r = R_1$.

To relate the value of R_1 to the fuel parameters at ignition, we assume that the DT shell—which, by the beginning of the main pulse, has been compressed to a thin layer with $\Delta r = R_1/A_c \ll R_1$—attains its implosion velocity U_{im} after it has been accelerated during the main pulse phase with a constant acceleration $g = U_{im}^2/R_1$ over one-half of its initial radius R_1. From this, we calculate

$$R_1[\text{mm}] = 0.136 A_c^{5/6} \frac{\alpha^{1/2} M_c^{1/3}}{U_{im}} \tag{22}$$

where A_c is the in-flight aspect ratio of the initially solid DT layer measured at the onset of the main pulse. M_c is in milligrams.

The Rayleigh–Taylor instability at the ablation surface imposes a limit on the in-flight aspect ratio of the ablator shell (A_a; as measured at the onset of the main pulse) [8,9], whose rupture we want to avoid. To relate A_a to A_c, we make the further assumption that, during the main pulse, the ablator material obeys the same equation of state, i.e. $P = K\alpha\rho^{5/3}$, as the compressed DT shell. This assumption is based on the observation that, on the one hand, the adiabatic index of low-Z elements becomes close to $\frac{5}{3}$ at pressures $P \simeq 100$ Mbar and, on the other hand, one would prefer to have no density jump at the fuel–ablator interface during the phase of fuel acceleration. A smooth density transition across the fuel–ablator interface enables one to combine the hydrodynamic stability of this interface with a maximum possible thickness of the ablator for a given value of its mass. It should be noted that the properties of realistic ablators may come close to but not quite reach the ideal case assumed here. As a consequence, we find that

$$A_c = A_a[(1 + M_a'/M_c)^{2/5} - 1] \approx A_a \tag{23}$$

provided that the ablator mass at the onset of the main pulse has its optimum value $M_a' \simeq (4–5)M_c$ [10]. Hence, in what follows, we do not distinguish between A_a and A_c, and assume an upper limit of $A_a = A_c = 30$ [9].

Taken alone, an upper bound on the in-flight aspect ratio A_c implies a lower limit on the driving pressure and an upper limit on the initial fuel radius R_1, but does not affect the scaling laws of Eqs. (19)–(21). The situation changes, however, when we take into account a limit on the radial convergence ratio. In our case, it is convenient to introduce two convergence ratios, i.e.

$$C_0 = \frac{R_0}{R_s}, \qquad C_1 = \frac{R_1}{R_s} \tag{24}$$

where R_s is the spark radius at ignition. Non-uniformities in the driving pressure associated with low angular modes impose an upper limit of 30–40 on possible values of C_0 [9]. For simplicity, we assume that this limit does not depend on other implosion parameters. From Eqs. (22) and (24), we calculate

$$C_1 = 0.622 \frac{A_c^{5/6}}{\xi_s} \left[\frac{(1-\xi_s^2)\phi_M}{\phi_E^{3/5}} \right]^{5/6} \tag{25}$$

$$C_0 = C_1 \left[1 + (1+b_{ac}) \left(\frac{11.2}{A_c} \right)^{5/2} \frac{U_{im}^3}{\alpha^{3/2}} \right]^{1/3} \tag{26}$$

In Eq. (26) it is assumed that the initial solid DT density is 0.224 g cm^{-3} and b_{ac} is the ratio between the initial ablator and the solid DT volumes. In numerical estimates, we used the value $b_{ac} = 1$, having assumed that, with allowance for the partial evaporation during the prepulse phase, the initial ablator mass is $M_a \simeq (7-10)M_c$, while its intial density is higher than the initial solid DT density by approximately the same factor. The two cnvergence ratios C_0 and C_1 practically coincide when the initial thickness $R_0 - R_1$ of the fuel-plus-ablator shell is small compared with its radius R_1, or, in other words, when the initial aspect ratio $A_0 = R_1/(R_0 - R_1) \gg 1$. It seems that, in the opposite limit of initially thick target shells, one should distinguish between C_0 and C_1.

A remarkable fact is that the ratio $C_1/A_c^{5/6}$ is a function of ξ_s only. For ignition at stagnation, fixed values of C_1 and A_c imply a fixed value of ξ_s. From this, we conclude that the scalings of Eqs. (19)–(21) are not affected by the constraints of the hydrodynamic instabilities and drive asymmetries when the inital aspect ratio of the fusion capsule $A_0 \gg 1$. In the opposite case of initially thick capsule shells—a typical case for ignition at low values of E_f—we should assume fixed values of A_c and C_0. As a consequence, ξ_s becomes an increasing function of the ratio U_{im}^2/α. Since Ψ_E in Eq. (20) is an increasing function of ξ_s (see Fig. 1), we obtain a weaker dependence of $E_{f,min}$ on α and U_{im} than that indicated by Eq. (21). Unfortunately, no well-defined power-law scaling can be established for $E_{f,min}$ and G_f^* in this region, partly because the second term in parentheses in Eq. (26) is not a power law.

This is clearly illustrated by Fig. 4, where three families of gain curves, calculated with the DEIRA code for three different values of α, are plotted. The only difference from the DEIRA curves in Fig. 3 is that each gain curve is now characterized by its own value of the fractional spark radius ξ_s, calculated from Eqs. (25) and (26), to keep $C_0 = A_c = 30$.

From Fig. 4, we infer that the scaling of $E_{f,min}$ with U_{im}, and of G_f^* with E_f changes from $E_{f,min} \propto U_{im}^{-3.6}$ and $G_f^* \propto E_f^{0.78}$ for $\alpha = 1$ to $E_{f,min} \propto U_{im}^{-5.9}$ and $G_f^* \propto E_f^{0.44}$ for $\alpha = 4$. Also, the scaling of $E_{f,min}$ with α changes from $E_{f,min} \propto \alpha^{2.3}$ for $U_{im} = 3 \times 10^7$ cm s^{-1} to $E_{f,min} \propto \alpha^{1.4}$ for $U_{im} = 5 \times 10^7$ cm s^{-1}. To compare these results with the Livermore scaling, it should first be noted that, in different Livermore publications, the reader finds rather different formulas: $E_{f,min} \propto \alpha^3 U_{im}^{-6}$ in Ref. [11], $E_{f,min} \propto \alpha^4 U_{im}^{-5}$ in Ref. [7] $E_{f,min} \propto \alpha^{1.5} U_{im}^{-5}$ in Ref. [1]; the scaling of $G_f^* \propto E^{2/3}$ in refs. [7,11] to $G_f^* \propto E^{0.73}$ in refs. [1,12]. In light of the above discussion, the most natural explanation for such a scatter would be that the Livermore results refer to initially thick shells, for which no well-defined power-law scaling can be established in general. A reasonable agreement between the predictions of the present model and the most recent scaling quoted by Lindl [1] is observed for values of α somewhere between 1 and 2, and $U_{im} \simeq 4 \times 10^7$ cm s^{-1}.

Acknowledgements

I appreciate a number of stimulating discussions with J. Meyer-ter-Vehn. This work was supported by the INTAS Grant 93-251.

References

[1] J.D. Lindl, Nuovo Cim. 106A (1993) 1467–1487.
[2] J. Meyer-ter-Vehn, Nucl. Fusion 22 (1982) 561–565.
[3] M. Murakami and Meyer-ter-Vehn, Nucl. Fusion 31 (1991) 1315–1331.
[4] S. Atzeni, Particle Accel. 37–38 (1992) 495–503
[5] J. Meyer-ter-Vehn, M. Basko, R. Ramis and A. Rickert, Nuovo Cim. 106A (1992) 1883–1892.
[6] M.M. Basko, Nucl. Fusion 35 (1995) 87–99.
[7] J.D. Lindl, R.L. McCrory and Campbell, Phys. Today 45 (1992) 32–40.
[8] C.P. Verdon, R.L. McCrory, R.L. Morse, G.R. Baker, D.I. Meiron and S.A. Orszag, Phys. Fluids 25 (1982) 1653–1668.
[9] J.D. Lindl, in Proc. Course and Workshop Inertial Confinement Fusion, 1988, Editrice Compositori, Bologna, 1989 pp. 595–630.
[10] M. Murakami and K. Nishihara Jpn. J. Appl. Phys. 26 (1987) 1132–1145.
[11] J.D. Lindl, in From Fusion to Light Surfing (Lectures on Plasma Physics Honoring John M. Dawson), Addison-Wesley, Redwood City, CA, 1991, pp. 177–190.
[12] E. Storm, et al., in Proc. 13th Int. Contion Plasma Physics and Controlled Nuclear Fusion Research, Washington, DC, 1990, Vol. 3, IAEA, Vienna, 1991 pp. 99–111.